31st Congress of the International Council of the Aeronautical Sciences

Belo Horizonte, Brazil; September 09-14, 2018

HIGHER FIDELITY TRANSONIC AERODYNAMIC MODELING IN PRELIMINARY AIRCRAFT DESIGN

Crovato A.* , **Dimitriadis G.*** , **Terrapon V.E.***

* **Universite de Liege, Belgium**

Keywords: *Field Panel Method, Computational Fluid Dynamics, Transonic aerodynamics, Aeroelasticity, Preliminary aircraft design*

Abstract

There is a consensus in the aerospace research community that future aircraft will be more flexible and their wings will be more highly loaded. While this development is likely to increase aircraft efficiency, it poses several aeroelastic questions. Current aeroelastic tailoring practice for early preliminary aircraft design relies on linear aerodynamic modeling, which is unable to predict shocks and boundary layers. The objective of this research is to enhance the linear aerodynamic modeling methodology, thus allowing fast and reliable aerodynamic loads prediction for aeroelastic computations. First, the different levels of fidelity of aerodynamic modeling that can be used in aircraft design are reviewed and compared on benchmark test cases. A Field Panel Method is subsequently developed and implemented. Preliminary results are presented and possible future enhancements are detailed.

1 Introduction

In the on-going effort to build more efficient aircraft, the minimization of the structural weight and the maximization of the aerodynamic efficiency usually lead to the design of very flexible and highly loaded composite wings. Aeroelasticity thus plays an increasingly important role in preliminary aircraft design. Since aeroelastic computations are performed early in the design process and involve the coupling of both aerodynamics and structural mechanics, the computational cost of the solution techniques must be kept as low as possible. The most widely used aerodynamic solver is thus the panel method, which relies on the linear potential equation. It is therefore unable to predict shocks appearing in the transonic flight regime. The objective of this research is to find a suitable aerodynamic model and develop a numerical tool to solve it. The different levels of fidelity used in aerodynamic modeling will first be briefly reviewed and compared on benchmark cases, showing that the nonlinear potential model is suitable for preliminary aircraft design computations. An implementation of the Field Panel Method will then be presented and its reliability, accuracy and current limitations will be assessed on test cases. Finally, possible enhancement will be discussed.

2 Levels of fidelity and methods

In this section, the different models for steady compressible flows commonly used in industry will be briefly explained.

2.1 Models

The highest level of fidelity considered in this research is the Reynolds-Averaged Navier-Stokes (RANS) equations:

$$\frac{\partial}{\partial x_j}(\rho\bar{u}_j) = 0,$$
$$\rho\bar{u}_j\frac{\partial\bar{u}_i}{\partial x_j} = -\frac{\partial\bar{p}}{\partial x_i} + \mu\frac{\partial^2\bar{u}_i}{\partial x_j^2} + \frac{\mu}{3}\frac{\partial^2\bar{u}_j}{\partial x_i\partial x_j} - \frac{\partial}{\partial x_j}(\rho\overline{\tilde{u}_i\tilde{u}_j}), \tag{1}$$

where ρ is the density, $\bar{\mathbf{u}}$ the mean velocity, $\tilde{\mathbf{u}}$ the fluctuation velocity, p the pressure and μ, the dynamic viscosity.
The unclosed Reynolds stress in Eq. 1 is computed using the Spalart-Allmaras turbulence model [1], which is commonly used for aeronautical flows.
The Euler equations are the inviscid version of the Navier-Stokes equations. They are obtained by neglecting the shear stress term,

$$\begin{aligned}
&\frac{\partial}{\partial x_j}(\rho u_j) = 0,\\
&\rho u_j\frac{\partial u_i}{\partial x_j} = -\frac{\partial p}{\partial x_i},\\
&\frac{\partial}{\partial x_j}(u_j(E+p)) = 0,\\
&E = \rho e + \frac{1}{2}\rho u_j^2,\\
&e = c_v T,\\
&p = \rho RT,
\end{aligned} \tag{2}$$

where E is the total energy, e is the specific energy, T is the temperature and c_v is the specific heat capacity at constant volume.
The Full Potential Equation (FPE) assumes that the flow is inviscid, isentropic and irrotational. Since the entropy produced across a shockwave is proportional to $(M-1)^3$, the isentropicity assumption is usually considered valid as long as the maximum Mach number in front of a shockwave is less than 1.3. The FPE is obtained by representing the irrotational velocity field as the gradient of a scalar potential, ϕ,

$$\begin{aligned}
&\partial_i(\rho\partial_i\phi) = 0\\
&\rho = \rho_\infty\left[1 + \frac{\gamma-1}{2}M_\infty^2\left(1-(\partial_i\phi)^2\right)\right]^{\frac{1}{\gamma-1}}.
\end{aligned} \tag{3}$$

The Linear Potential Equation (LPE) further assumes that the flow is smooth and is obtained by linearizing the Full Potential Equation,

$$(1-M_\infty^2)\frac{\partial^2\phi}{\partial x^2} + \frac{\partial^2\phi}{\partial y^2} + \frac{\partial^2\phi}{\partial z^2} = 0, \tag{4}$$

where M_∞ is the (subsonic) freestream Mach number.

The Boundary Layer Equations (BLE) are a particularization of the Navier-Stokes equations. They are usually solved in integral form and used in conjunction with the LPE, FPE or Euler equations to account for the viscosity and model the boundary layer. More details about the formulation can be found in Drela's paper [2].
The Flat Plate Analogy (FPA) is an empirical formula assuming that the friction drag of a wing equals the drag of a flat plate of similar wetted area in an equivalent flow. In this work, the friction coefficient C_f was computed assuming that the flow was fully turbulent around the wing (Re is the Reynolds number),

$$C_f = \frac{0.074}{\mathrm{Re}^{0.2}}. \tag{5}$$

2.2 Methodologies

The Euler and RANS solutions were computed by `su2`, an open-source finite-volume solver developed at Stanford University by Palacios et al. [3]. The related meshes were created in `ANSYS ICEM`. The full potential solutions, inviscid or coupled to the BLE, were computed by `TRANAIR`, a finite-element code developed in 1992 by Johnson et al. [4] at Boeing and currently owned by Calmar Research. Finally, the linear potential solution was obtained by `PANAIR`, a higher-order panel method also developed at Boeing by Carmichael & Erickson [5] in 1981[1].

[1] The code is now open-source.

3 Aerodynamic predictions on benchmark cases

In this section, the aforementioned models and methods will be compared on benchmark cases.

3.1 Onera M6 wing

The Onera M6 is a wing featuring a low aspect ratio of 3.8, a moderate sweep of 30° and a taper ratio of 0.56. The wing has been simulated at Mach 0.84 and an angle of attack α of 3°.
Figure 1 shows the pressure distributions obtained with the different models as well as experimental data gathered by Schmitt & Charpin [6], along the chord at two different spanwise stations. The first one is located near the mean aerodynamic chord while the second is located outboard and features a double shock.
Figure 1a confirms that the linear potential model does not represent the actual physics of transonic flows since it is unable to predict shocks. The inviscid models such as the Euler and the full potential equations are found to correctly represent the physics even though they predict stronger shocks. Finally, the viscous models give an accurate prediction, although a small difference in the shock location and strength is still observed. When the physics is more complex, as depicted in Figure 1b, the FPE, corrected by the BLE or not, is not as accurate as higher-fidelity computations. In particular, the first shock is significantly smeared. However, even the RANS solution shows a significant difference in the first shock location.
Figure 2 shows the spanwise lift and moment distributions obtained with the different models compared to experimental data [6]. The quarter-chord of each wing section has been chosen as the reference point for the moment computation.
Figure 2a shows that every model predicts a similar lift curve, with small differences in magnitude. This result is not surprising as the geometry of the wing is simple. On the other hand, Figure 2b shows that the linear potential equation fails to predict the correct trend of twisting moment across the wing span.

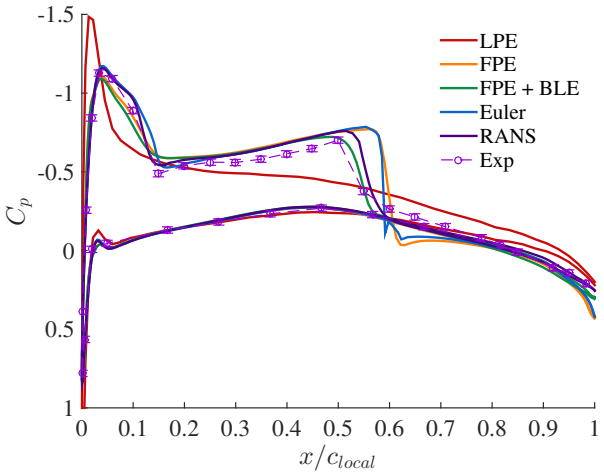

(a) $y/b = 0.44$.

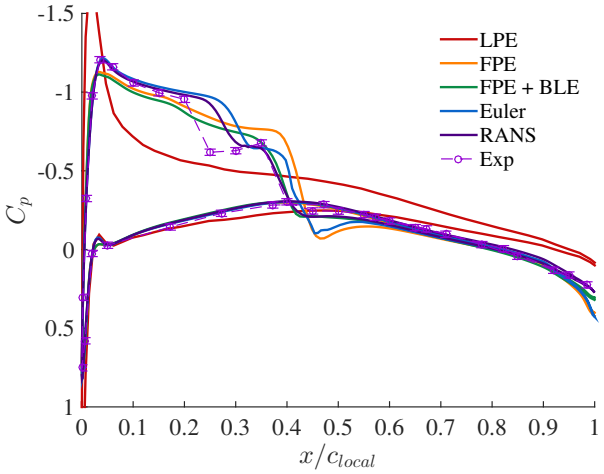

(b) $y/b = 0.8$.

Fig. 1 : Pressure distribution along the chord at two different spanwise locations for the Onera M6 wing at $M = 0.84$ and $\alpha = 3°$ obtained from different numerical approaches and compared to the experimental data [6].

The surface pressure and friction drag components of the Onera M6 wing are shown in Figure 3. The pressure drag components given by the different models are similar, except for the linear potential equation which misses the shock and the associated wave drag production. The small differences in the pressure drag predictions between the other four models are due to the differences in lift (which give different lift-induced drag components) and to the difference in boundary layer modeling. Furthermore, the Flat Plate

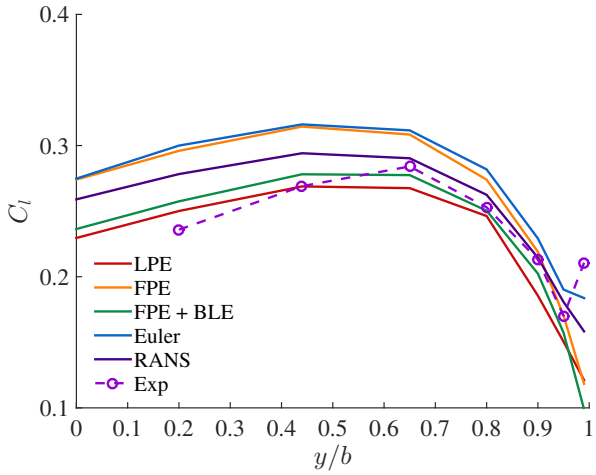

(a) C_l.

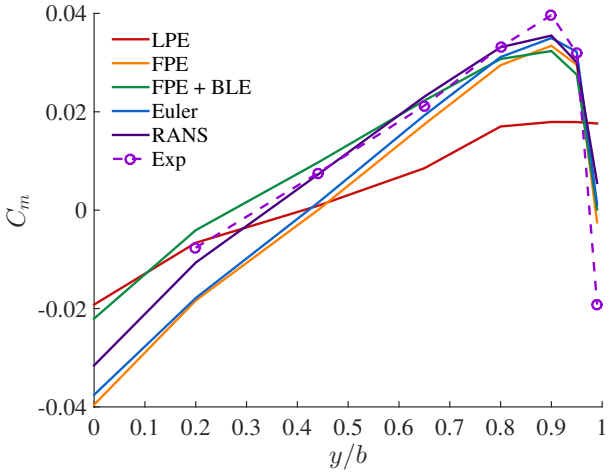

(b) C_m.

Fig. 2 : Sectional lift and quarter-chord moment coefficients along the span for the Onera M6 wing at $M = 0.84$ and $\alpha = 3°$ obtained from different numerical approaches and compared to the experimental data [6].

Analogy predicts the same amount of friction drag as the BLE and the RANS equations. In cruise conditions (low angle of attack and moderate lift production), where the boundary layer remains mostly attached, the FPA can thus be used to predict the friction drag.

Finally, the computational times, noted as number of CPU core times time per CPU cores, needed by the different codes are: a) LPE: 1×5s, b) FPE: 1×600s, c) FPE+BLE: 1×900s, d) Euler: 6×3h, e) RANS: 32×24h.

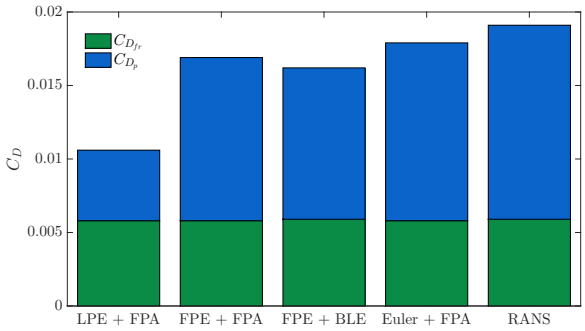

Fig. 3 : Comparison of the predicted friction and pressure drag contributions between the different numerical approaches for the Onera M6 at $M = 0.84$ and $\alpha = 3°$.

3.2 Embraer Benchmark Wing

The comparison of the different numerical approaches is repeated for the Embraer Benchmark wing (EBW2) that is more representative of an actual aircraft wing. Unfortunately, no experimental data is available for this case. The EBW2 is a double planform, large aspect ratio, swept, twisted and tapered wing. The wing has been simulated at typical cruise condition: Mach 0.78 and altitude of 35000ft. For each calculation, the angle of attack is adjusted such that the resulting lift coefficient is equal to $C_L = 0.47$.

At cruise speed, the flow is supercritical, *i.e.* a supersonic region is embedded in the subsonic flow and terminated by a shock. In this case, the shock is weak and located at $\sim 60\%$ of the local chord, as depicted in Figure 4. The linear potential model again fails to properly represent the flow, since it does not capture the shock. Higher-fidelity but inviscid models, such as the full potential and the Euler equations, properly capture the physics of the flow, but tend to predict the shock location too far downstream. When the models take the viscous effects into account, the shock location moves forward.

At this moderate freestream Mach numbers, all models give approximately the same lift distribution as shown in Figure 5a. Small differences can

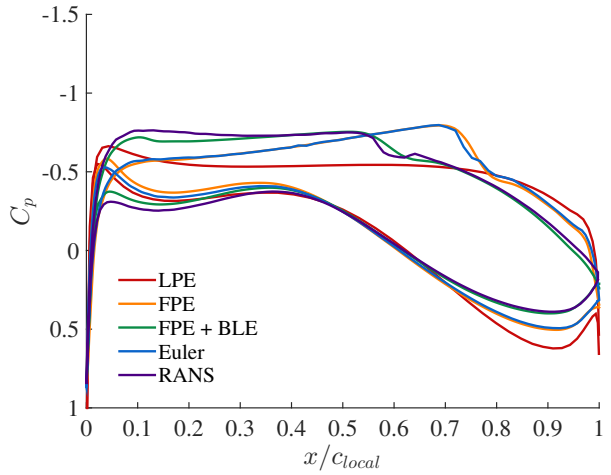

Fig. 4 : Comparison of the predicted pressure distributions between the different numerical approaches along the mean aerodynamic chord of the EBW2 at $M = 0.78$ and $C_L = 0.47$ ($y/b = 0.406$).

be observed near the kink, located at $y/b = 0.36$, where the wing planform changes. Regarding the quarter-chord moment coefficient (Fig. 5b), the models predict the same trend, except the linear potential equation which misses the local minimum at the kink. Inviscid models tend to predict lower moment coefficients than viscous models because they do not take into account the boundary layer (which causes a change in lift production and thus, in angle of attack required to produce the same amount of lift). The angles of attack given by the different models are: a) LPE: $-1.6°$, b) FPE: $-1.8°$, c) FPE+BLE: $-0.7°$, d) Euler: $-1.7°$, e) RANS: $0.3°$.

The surface pressure and friction drag components of the EBW2 wing are shown in Figure 6. The FPA gives again a good estimation of the friction drag. Furthermore, the pressure drag components obtained by the different methods are comparable. The small differences are due to the solvers or to the different boundary layer modeling techniques.

Finally, the computational time, noted as number of CPU core times time per CPU core, needed by the different codes are: a) LPE: 1×5s, b) FPE: 1×400s, c) FPE+BLE: 1×900s, d) Euler: 6×3h, e) RANS: 32×24h.

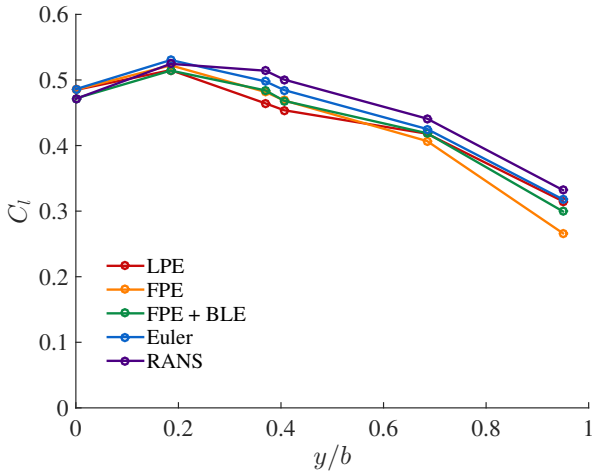

(a) C_l.

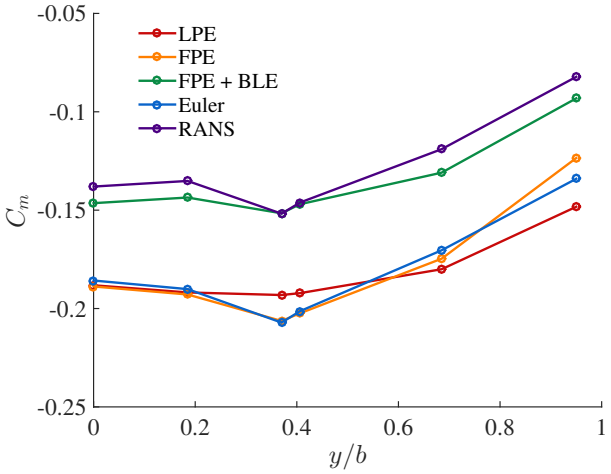

(b) C_m.

Fig. 5 : Comparison of the predicted sectional lift and quarter-chord moment coefficients between the different numerical approaches along the span of the EBW2 at $M = 0.78$ and $C_L = 0.47$.

3.3 Discussion

The flow around two wings, the Onera M6 and the Embraer Benchmark Wing, was modeled using several levels of fidelity. At typical cruise flight conditions, the flow is supercritical and weak shocks appear on the wing surface. Consequently, the LPE fails to predict the pressure distribution and the wave drag. On the other hand, the Euler and RANS equations give accurate solutions but at a high computational cost. Since the FPE+BLE gives predictions compa-

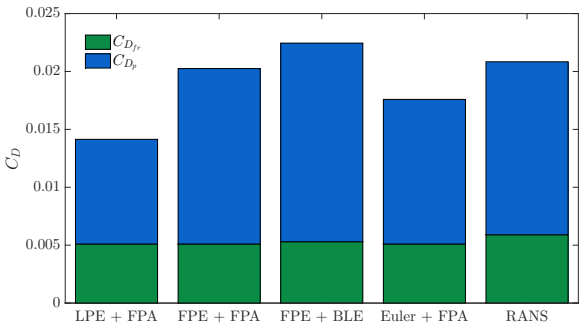

Fig. 6 : Comparison of the predicted friction and pressure drag contributions between the different numerical approaches for the EBW2 at $M = 0.78$ and $C_L = 0.47$.

rable to the RANS equations for a fraction of the computational cost, it can be regarded as the most efficient model for aeroelastic computation in preliminary aircraft design. In an optimization process, such as aeroelastic tailoring, which involves the repeated computation of the aerodynamic loads as the structure is being optimized, the *fast* inviscid FPE could be used for a fixed number of aeroelastic iterations before being recalibrated by one *more accurate* viscous FPE+BLE solution.

4 Field Panel Method

Different ways of solving the promising Full Potential Equation have been investigated. The Field Panel Method (FPM) has been chosen over traditional Finite Element/Volume methods because the FPM is a direct extension of the panel method, and is able to directly provide the Aerodynamic Influence Coefficients needed for optimization processes. Moreover, it does not require a body-fitted mesh and can be easily coupled to the BLE. The FPM (and the underlying panel method) has been implemented following the ideas of Katz and Plotkin [7] and Gebhardt et al. [8].

4.1 Theory

The main idea behind the Field Panel Method is to rewrite the nonlinear Full Potential Equation as a Poisson equation containing a linear part and a nonlinear term,

$$\begin{aligned} &\nabla \cdot (\nabla \phi) = \sigma, \\ &\sigma = \nabla \cdot \left[(1 - \frac{\rho}{\rho_\infty}) \nabla \phi \right], \\ &\rho = \rho_\infty \left[1 + \frac{\gamma - 1}{2} M_\infty^2 \left(1 - (\nabla \phi)^2 \right) \right]^{\frac{1}{\gamma - 1}}. \end{aligned} \tag{6}$$

The linear part, which is essentially the incompressible Linear Potential Equation, is solved by the panel method and iteratively corrected by the nonlinear source term. The first equation of (6) can be transformed using Green's theorem into,

$$\begin{aligned} \phi(x,y,z) = \phi_\infty &\underbrace{- \frac{1}{4\pi} \int_{S_B} \left[\tau \frac{1}{r} - \mu \mathbf{n} \cdot \nabla (\frac{1}{r}) \right] dS}_{\varphi_b} \\ &\underbrace{- \frac{1}{4\pi} \int_V \left[\sigma \frac{1}{r} \right] dV}_{\varphi_f}, \end{aligned} \tag{7}$$

where r is the distance defined by $\sqrt{x^2 + y^2 + z^2}$, ϕ_∞ is the freestream potential given by $U_{x,\infty} x + U_{y,\infty} y + U_{z,\infty} z$, τ are the surface source singularities, μ are the doublet surface singularities, σ are the volume source singularities, and $\mathbf{n}$ is the surface unit normal vector.

Equation 7 shows that the total potential can be written as a superposition of a linear potential φ_b and a nonlinear source term σ. The panel method is used to obtain the linear potential. The body is discretized into panels on which doublet and source singularities are superimposed. These singularities are then computed by enforcing the impermeability boundary condition (Eq. 9) at the surface of the body. To represent the source term, a rectangular parallelepipedic volume enclosing the nonlinearities in the flow around the geometry is defined. This volume is then di-

vided into uniform cells to form a Cartesian, non-body-conforming, grid. Each cell is treated as a field panel containing a constant source singularity distribution of strength σ. These singularities are iteratively computed according to the second equation in 6, in which the perturbation potential in the field φ_f is computed by the AIC matrices derived from Equation 7,

$$\varphi_f = \mathbf{A}_f\mu + \mathbf{B}_f\tau + \mathbf{C}\sigma, \tag{8}$$

where the vector of surface singularities μ and τ are updated by the panel method. To close the iterative procedure and to respect the impermeability boundary condition, the surface source singularities must include the normal component of the freestream velocity as well as the normal component of the velocity induced by the field sources. The new boundary condition reads,

$$\nabla\varphi_b \cdot \mathbf{n} = -\nabla(\phi_\infty + \varphi_f) \cdot \mathbf{n}. \tag{9}$$

When the flow is supersonic, the information travels at the speed of sound in the fluid and thus cannot propagate upstream. Consequently, the equation, elliptic in a a subsonic flow, becomes hyperbolic in a supersonic flow. In the finite difference/element/volume methods, this change of physics should be reflected by a change in the discretization scheme for the derivatives. In the present work, three techniques have been tested: derivative upwinding, artificial density and artificial viscosity. Since they all gave similar results the artificial viscosity technique has been retained due to its simplicity. As shown by Rottegermann and Wagner [9], it consists in adding a term directly to the field sources,

$$\tilde{\sigma} = \sigma + \lambda\frac{\partial\sigma}{\partial s}\Delta s, \tag{10}$$

where λ is a switching function depending on the local Mach number, s is the local flow direction and Δs is the local mesh size.

4.2 Full solution procedure

This section describes the solution procedure currently implemented. To setup a simulation solely depending on the Mach number and angle of attack, the field variables have been normalized by setting the magnitude of the freestream velocity to $V_\infty = 1$.

Initialization

After the geometry preprocessing, the matrices containing the influence coefficients are computed: body to body ($\mathbf{A}$ and $\mathbf{B}$), field to field ($\mathbf{C}$), body to field ($\mathbf{A}_f$ and $\mathbf{B}_f$) and field to body ($\mathbf{C}_{\mathbf{x},b}$, $\mathbf{C}_{\mathbf{y},b}$, $\mathbf{C}_{\mathbf{z},b}$). All the relevant variables (like the field sources $\tilde{\sigma}$ and the velocity induced by the field sources $u_{n,\sigma}$) are also initialized to zero.

Step 1 - Surface sources

The first step of the iterative process consists in setting the surface source singularities τ to $-(\mathbf{V}_\infty \cdot \mathbf{n} + u_{n,\sigma})$ so that they include the non-lifting normal velocity component, according to Eq. 9.

Step 2 - Surface doublets

The next step consists in solving the linear system of equations $\mathbf{A}\mu + \mathbf{B}\tau = 0$ to obtain the surface doublet singularities, μ.

Step 3 - Field variables

The next step consists in computing the different field variables. The total potential in the field is computed from $\phi_f = \phi_\infty + \mathbf{A}_f\mu + \mathbf{B}_f\tau + \mathbf{C}\tilde{\sigma}$, and differentiated with finite differences to obtain the total velocity in the field $\mathbf{V}_f$. The speed of sound a, the Mach number M and the density ratio $\frac{\rho}{\rho_\infty}$ are then computed using the isentropic relations (γ is the specific heat ratio for air):

$$\begin{aligned} a^2 &= a_\infty^2 + \frac{\gamma-1}{2} - \frac{\gamma-1}{2}{\mathbf{V}_f}^2, \\ M &= \frac{V_f}{a}, \\ \frac{\rho}{\rho_\infty} &= \left[1 + \frac{\gamma-1}{2}M_\infty^2\left(1 - {\mathbf{V}_f}^2\right)\right]^{\frac{1}{\gamma-1}}. \end{aligned} \tag{11}$$

Step 4 - Field sources

The next step consists in updating the field source singularities according to $\sigma = \nabla\left(\frac{\rho}{\rho_\infty}\right) \cdot \mathbf{V}_f$. The

artificial viscosity is then added using Eq. 10.

Step 5 - Boundary condition update

The normal component of the velocity induced by the field sources can now be recomputed as $u_{n,\sigma} = [\mathbf{C}_{\mathbf{x},\mathrm{b}}\tilde{\sigma}, \mathbf{C}_{\mathbf{y},\mathrm{b}}\tilde{\sigma}, \mathbf{C}_{\mathbf{z},\mathrm{b}}\tilde{\sigma}] \cdot \mathbf{n}$

Step 6 - Stopping criterion

Steps 1 to 5 are repeated until convergence. The stopping criterion is defined as, $\max|\tilde{\sigma}^{\mathrm{n}} - \tilde{\sigma}^{\mathrm{n}-1}| < \varepsilon$, where n is the iteration counter and ε is a user-defined tolerance, typically 10^{-6}.

Finalization

The last step is to compute the surface velocity and the pressure coefficient. The surface velocity is the sum of the freestream velocity $\mathbf{V}_\infty$, the surface perturbation velocity $\mathbf{u}_\mathrm{b}$ and the field perturbation velocity $\mathbf{u}_\mathrm{f}$. The latter has already been calculated to update the boundary condition. The surface perturbation velocity can be computed by differentiating the potential on the surface with finite differences. If l, m and n are the axes of the frame attached to a panel, then

$$\begin{aligned} u_{l,\mathrm{b}} &= -\frac{\partial \mu}{\partial l} \\ u_{m,\mathrm{b}} &= -\frac{\partial \mu}{\partial m} \\ u_{n,\mathrm{b}} &= \tilde{\sigma}. \end{aligned} \tag{12}$$

The resulting velocity vector is then rotated to the global axis and used to compute the total surface velocity,

$$\mathbf{V}_\mathrm{b} = \mathbf{V}_\infty + \mathbf{u}_\mathrm{b} + \mathbf{u}_\mathrm{f}. \tag{13}$$

The pressure coefficient can subsequently be computed from,

$$C_p = \frac{2}{\gamma M_\infty^2}\left\{\left[1 + \frac{\gamma-1}{2}M_\infty^2(1-V_\mathrm{b}^2)\right]^{\frac{\gamma}{\gamma-1}} - 1\right\}. \tag{14}$$

5 Results

This section illustrates flow solutions obtained by the implement Field Panel Method.

5.1 Subcritical flow

The compressible flows around a rectangular NACA0012 (aspect ratio of 10) and the Onera M6 wings are first analyzed. The angle of attack of the NACA0012 is set to 0° to obtain a nonlifting flow while the angle of attack of the M6 is set to 2°. The Mach number is chosen so that the flow remains subcritical for both wings.
Figure 7 shows the pressure distribution around the mean aerodynamic chord (MAC), which is measured at the aerodynamic center of an half wing, of both wings. Globally, the FPM shows excellent agreement with `TRANAIR` except near the suction peak, which is underestimated. The FPM solution is more accurate than the result obtained using the linearized potential flow equation (`PANAIR`).

5.2 Supercritical flow

The Mach number is now chosen so that the flow becomes supercritical for same two wings. The angle of attack of the NACA0012 is set to 0° to obtain a nonlifting flow while the angle of attack of the M6 is set to 3°.
Figure 8 shows the pressure distribution around both wings. When the flow exhibits a shock, the accuracy of the method is degraded. Figs. 8a and 8b both show that the present implementation of the FPM tends to predict a shock that is smeared and displaced upstream compared to `TRANAIR`'s full potential solution. Fig. 8b also shows that the present solution follows the same trend as the solution obtained by Gebhardt et al. [8]. Even if the FPM solution shows significant improvement over the linear potential solution predicted by `PANAIR`, this is at the cost of the computational time and memory required to compute and store the AICs. A Fast Multipole Method could be implemented to reduce the computational requirements for N^2 to N, where N is the degree of freedom. The FPM would then be possibly faster than existing Finite Element/Volume methods, even for transonic flow computations.

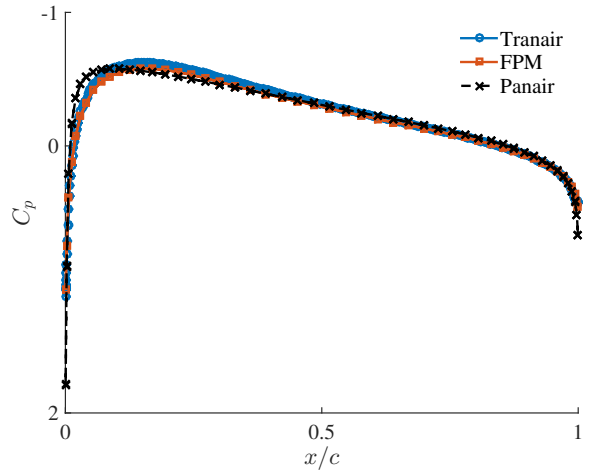

(a) NACA0012: $\alpha = 0°$, $M = 0.7$.

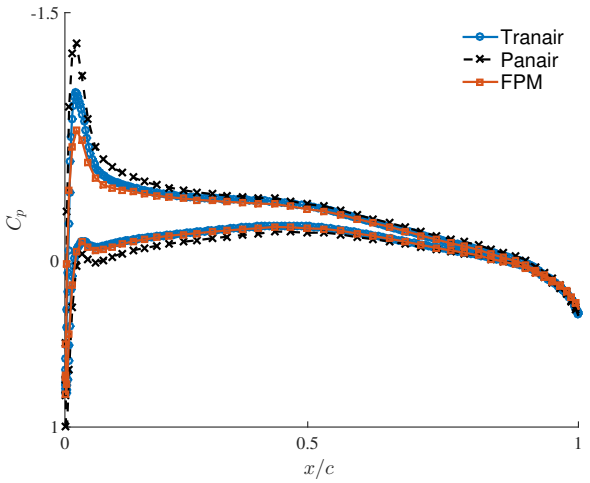

(b) Onera M6: $\alpha = 2°$, $M = 0.65$.

Fig. 7 : Pressure distribution around the MAC of NACA0012 and Onera M6 at subcritical speed.

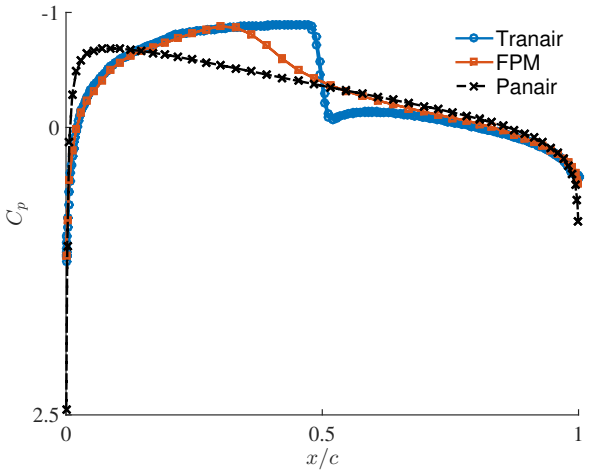

(a) NACA0012: $\alpha = 0°$, $M = 0.8$.

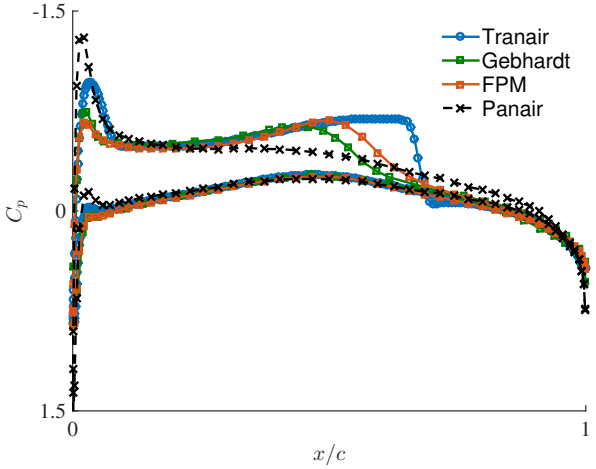

(b) Onera M6: $\alpha = 3°$, $M = 0.84$.

Fig. 8 : Pressure distribution around the MAC of NACA0012 and Onera M6 at supercritical speed.

6 Conclusion

In the context of fast aeroelstic computations for preliminary aircraft design, different levels of fidelity commonly used in the aerospace industry have been compared on two benchmark wings. A Field Panel Method was subsequently developed and implemented to solve the Full Potential Equation, and quickly model transonic flows. For a subcritical flow, the agreement between the different solutions is excellent, except near the pressure peak, where the pressure tends to be underestimated by the Field Panel Method. This could be due to insufficient local grid refinement. When the flow is supercritical, the solution is improved compared to the linear potential prediction but the captured shock tends to be displaced upstream and smeared. In order to reduce the computational requirements for transonic flows, a Fast Multipole Method could be implemented. This would enable the FPM to remain competitive with the Panel Method and allow it to be used in aeroelastic tailoring for preliminary aircraft design.

7 Acknowledgment

This research is funded by the Fonds de la Recherche Scientifique de Belgique (F.R.S.-FNRS) through a FRIA grant fellowship. The authors would also like to gratefully acknowledge the aerospace company Embraer S.A., who provided the wing model. Computational resources have been provided by the Consortium des Équipements de Calcul Intensif (CÉCI), funded by the Fonds de la Recherche Scientifique de Belgique (F.R.S.-FNRS) under Grant No. 2.5020.11.

References

[1] Spalart P.R. and Allmaras S.R. A one equation turbulence model for aerodynamic flows. *AIAA journal*, Vol. 94, 1992.

[2] Drela M. Three-Dimensional Integral Boundary Layer Formulation for General Configurations. *AIAA journal*, 2013.

[3] Palacios F. and Colonno M.R. and Aranake A.C. and Campos A. and Copeland S.R. and Economon T.D. and Lonkar A.K. and Lukaczyk T.W. and Taylor T.W. and Alonso J.J. Stanford University Unstructured (SU2): An open-source integrated computational environment for multi-physics simulation and design. *AIAA journal*, Vol. 287, 2013.

[4] Johnson F.T. and Samant S.S. and Bieterman M.B. and Melvin R.G. and Young D.P. and Bussoletti J.E. and Hilmes C.L. TranAir: A Full-Potential, Solution-Adaptative, Rectangular Grid-Code for Predicting Subsonic, Transonic, and Supersonic Flows About Arbitrary Configurations, 1992.

[5] Carmichael R.L. and Erickson L.L. Panair: A higher order panel method for predicting subsonic or supersonic linear potential flows about arbitrary configurations, 1981.

[6] Schmitt V. and Charpin F. Pressure distributions on the ONERA-M6-wing at transonic Mach numbers. *Experimental data base for computer program assessment*, Report of the Fluid Dynamics Panel Working Group 04, AGARD AR 138, May 1979.

[7] Katz J. and Plotkin A. *Low-Speed Aerodynamics*. 2nd edition, Cambridge University Press, 2001.

[8] Gebhardt L. and Fokin D. and Lutz T. and Wagner S. An Implicit-Explicit Dirichlet-Based Field Panel Method for Transonic Aircraft Design. *AIAA journal*, Vol. 40, pp 1-13, June 2002.

[9] Rottegermann A. and Wagner S. Cost Efficient Calculation of Compressible Potential Flow Around a Helicopter Rotor Including Free Vortex Sheet. *Aerodynamics and Aeroacoustics of Rotorcraf*, Berlin, Germany, October 1994.

Copyright Statement